Supporting Information

The thermodynamic origin for the structural transition pathway in metal oxide nanoparticles under acoustic shock excitation states

Sivakumar Aswathappa[1], Lidong Dai[1*], Sahaya Jude Dhas Sathiyadhas[2]

[1]School of Physics and Electronic Science, Guizhou Normal University, Guiyang, 550025, China

[2]Saveetha School of Engineering, Saveetha Institute of Medical and Technical Sciences, Saveetha University, Chennai, Tamil Nadu, 602105, India

Corresponding author: dailidong@vip.gyig.ac.cn, dailidong@gznu.edu.cn

Experimental section

Shock wave loading procedure

The required shock waves are generated by an in-house semiautomatic Reddy Tube which is capable of producing shock waves. It has three sections such as driver, driven and diaphragm sections. The driver and driven sections are made of seamless steel tubes of length 48 cm and 33 cm, respectively and both have the same inner diameter of 1.5 cm. Atmospheric air is used as the working substance for the required shock wave generation which is supplied by a tabletop mini 1 HP air compressor that has the capacity of 8 bars pressure storage. The diaphragm section separates the driver section and the driven section. Carbonless paper diaphragms are fed into the diaphragm section with the help of a motor. While the atmospheric air is being compressed into the driver section, at the critical pressure, the diaphragm is ruptured such that the shock wave is generated and moves along the driven section.

An indigenously developed semi-automatic Reddy tube has been used to generate the shock waves. In the present experiment, shock waves of Mach number 2.2 have been utilized possessing the dynamic transient pressure of 2 MPa and temperature 864 K. The shock waves from the driven section go on striking the sample which is located 1 cm away from the open end of the driven section. One end of the driver section is connected to the diaphragm section which has two pneumatic cylinders and the other end is connected to the compressor. The pressurized air is also utilized for the operation of pneumatic cylinders. Using the pressure controller of the driver section, we can control the input pressure range of the driver section and the schematic diagram is presented in **Fig. S1 (a, b).**

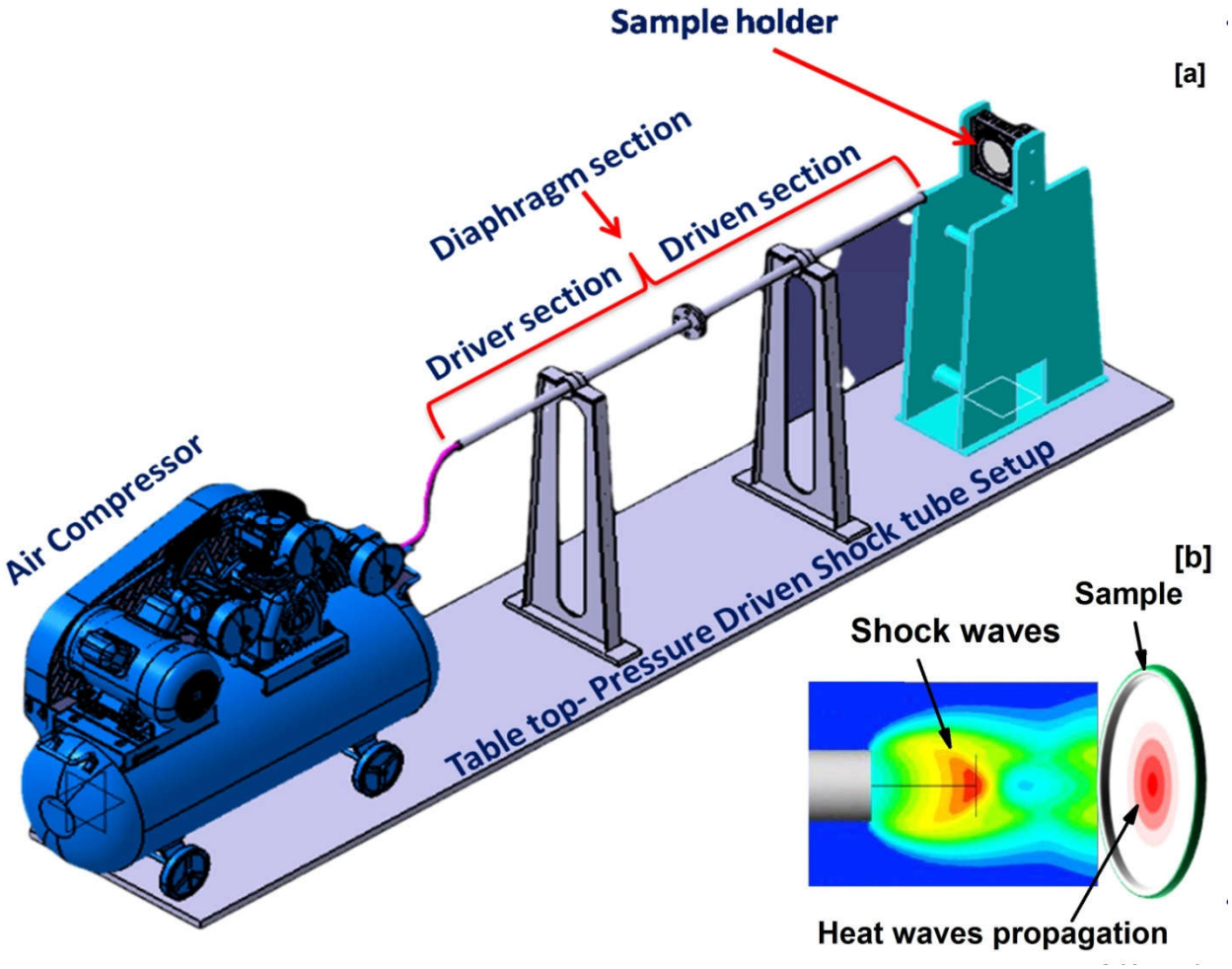

Fig. S1 (a) Schematic diagram of the table top pressure driven shock tube (b) shock propagation on the sample

Operation of the shock tube

Pressure of the air in the driver section is gradually increased by the air compressor until the diaphragm ruptures which leads to the generation of shock wave traveling along the axis of the driven section. The required numbers of test samples are to be placed one by one in the sample holder which is typically placed 1cm away from the open end of the driven section. Subsequently, required numbers of shock pulses are loaded on the respective test sample with an interval of 5 sec between each shock pulse. 100 number of shock pulse means that the sample is

exposed for 100 times by shock wave of a particular Mach number. After the completion of the shock wave loading experiment, the control and shock wave loaded samples are sent for analytical studies.

R-H relations

$$P2 = P1\left[1 + \frac{2\gamma}{\gamma + 1}(M^2 \quad 1)\right] (1)$$

$$\frac{T_2}{T_1} = \frac{P_2}{P_1}\left[\frac{\left(\frac{\gamma + 1}{\gamma \quad 1}\right) + \frac{P_2}{P_1}}{1 + \left(\frac{\gamma + 1}{\gamma \quad 1}\right)\frac{P_2}{P_1}}\right] \quad (2)$$

$$\frac{P_5}{P_2} = \frac{(3\gamma \quad 1)\frac{P_2}{P_1} - (\gamma \quad 1)}{(\gamma \quad 1)\frac{P_2}{P_1} + (\gamma + 1)} (3)$$

$$\frac{T_5}{T_2} = \frac{P_5}{P_2}\left[\frac{\left(\frac{\gamma + 1}{\gamma \quad 1}\right) + \frac{P_5}{P_2}}{1 + \left(\frac{\gamma + 1}{\gamma \quad 1}\right)\frac{P_5}{P_2}}\right] (4)$$

The initial fixed values are P_1=1 bar, γ=1.4 and T=300 K, where M- Mach number, P_5 and T_5 stand for the reflected transient pressure and temperature at the end of the driven tube, respectively.

Analytical experiments

Powder X-ray diffraction

The analysis of Powder X-ray diffraction (PXRD) [Rigaku – Smart Lab X-Ray Diffractometer, Japan- CuKα1 as the X-ray source (λ = 1.5407 Å), with the step precision of ± 0.001°] was performed over the diffraction angle from 10-90 degree. The high-power X-ray is 9 kW and focus type is line focus. Active area is 384 mm^2 (19.2×20 mm). Spatial resolution is 75 μm and Global count rate is 2.5×10^8 (1×10^6 cps/pixel). Efficiency of this technique with target material of Cu is 99 %. Highest flux X-ray source: PhotonMax, HyPix-3000 high energy resolution 2D detector, New CBO family, with fully automated beam switchable CBO-Auto and Various operando measurements with the new SmartLab Studio II.

Raman spectroscopy

We investigated the Raman spectra of the control and shocked samples using a Renishaw 2000 micro confocal Raman spectrometer coupled with a 532 nm argon ionic excitation source and laser source energy is 50 mW. The spectral frequency of this spectrometer is 100-3500 cm^{-1} and the spectral resolution is 0.75 cm^{-1} (FWHM) and the depth resolution is 2 mm (100 X objectives). Single-crystal silicon with a characteristic Raman peak at 520.0 cm^{1} was utilized to calibrate the Raman spectroscopy system prior to measurement. Raman spectra of the control and shocked SnO_2 NPs were gathered within the wavenumber range of 100 3500 cm^{1} in the backscattering geometry with the spectral resolution of 1.0 cm^{1} and the acquisition time was 120 secs. The laser spot size was 50 μm^2 and the optical microscope's objective lens was used such that an X50 long working distance objective lens (WD = 10.6 mm) was utilized and the value of numerical aperture was 0.5 while the Raman data was collected by Renishaw Wire 5.1

instrument control and the data acquisition software. We processed the obtained Raman spectra with a Lorentzian-type function in Origin 9.0 software to extract the Raman peak position and its corresponding FWHM.

Results

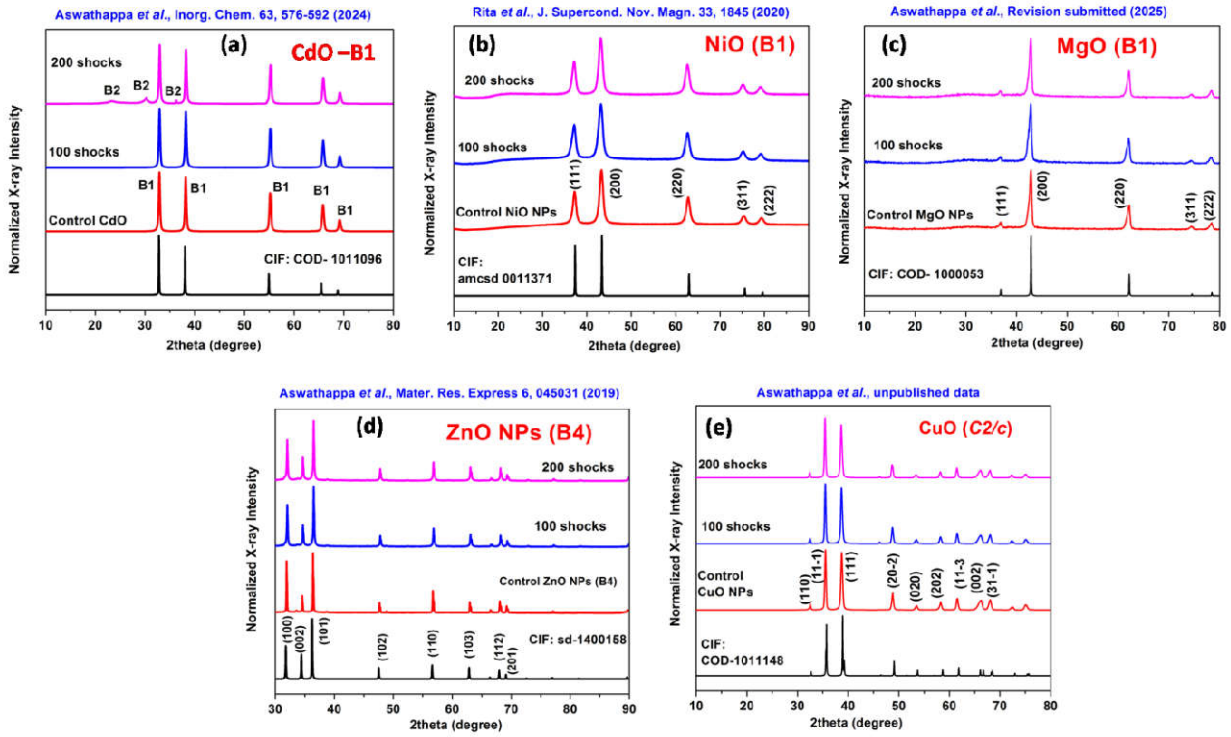

Fig. S2 Structural response of the control shocked AX type NPs (a) CdO, (b) NiO, (c) MgO, (d) ZnO and (e) CuO (Note: here all the published XRD data are reproduced with required permission)

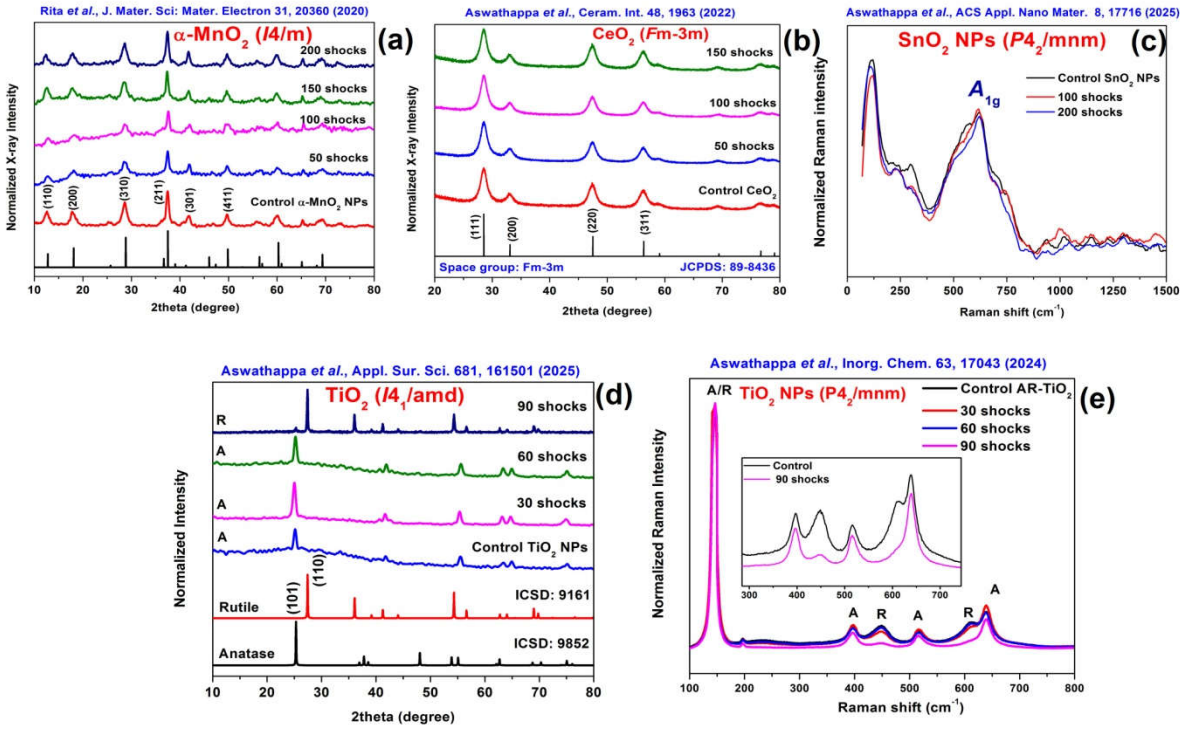

Fig. S3 Structural response of the control shocked AX_2 type NPs (a) α-MnO_2, (b) CeO_2, (c) SnO_2, (d) A-TiO_2 and (e) R-TiO_2 (Note: here all the published XRD and Raman data are reproduced with required permission)

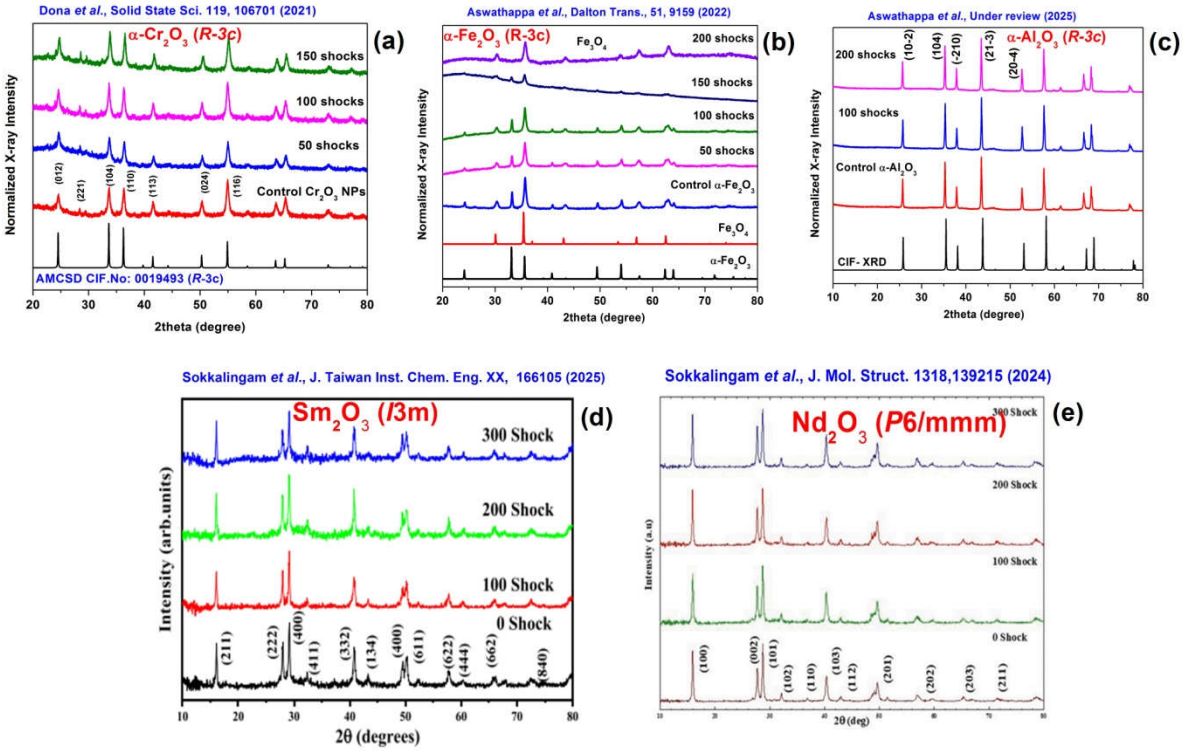

Fig. S4 Structural response of the control shocked A_2X_3 type NPs (a) α-Cr_2O_3, (b) α-Fe_2O_3, (c) α-Al_2O_3, (d) A-TiO_2 and (e) R-TiO_2 (Note: here all the published XRD data are reproduced with required permission)

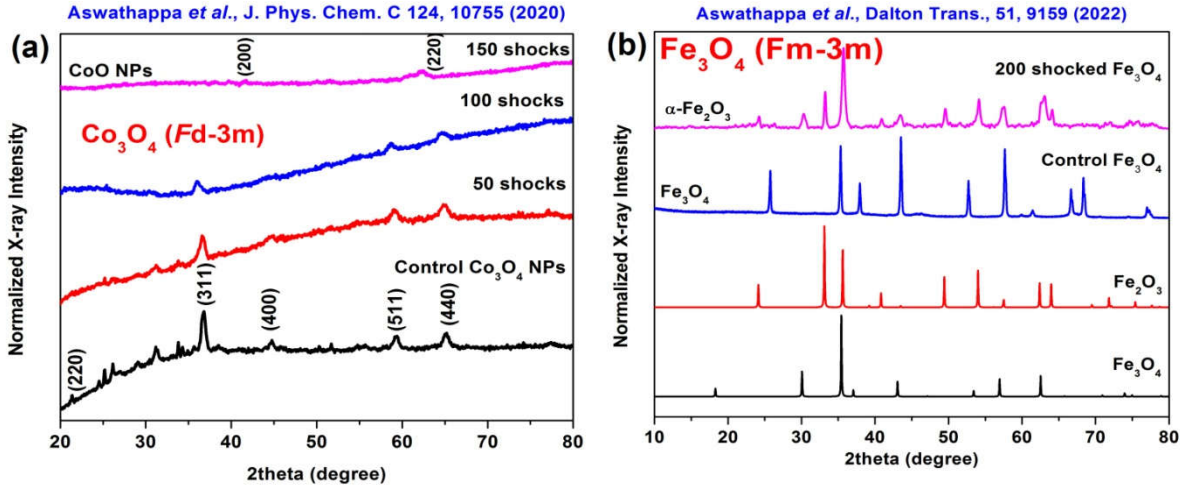

Fig. S5 Structural response of the control shocked A_3X_4 type NPs (a) Co_3O_4 (b) Fe_3O_4

(Note: here all the published XRD data are reproduced with required permission)

Table. 1 Thermal conductivity-dependent phase stability details of the control and shocked metal oxides NPs with respect to the number of shock pulses

S.NO	Materials	No. of shocks	Thermal conductivity ($Wm^{-1}K^{-1}$)	Transient pressure and temperature	Phase transition route	Phase transition route	Ref
1	A-TiO_2	90	1.5	2.0 MPa and 864 K	anatase to rutile	K-path	[1,2]
2	R-TiO_2	90	3.4	2.0 MPa and 864 K	rutile to anatase	-	[3]
3	Fe_3O_4	200	3.5	2.0 MPa and 864 K	Fe_3O_4- α-Fe_2O_3	K-path	[4]
4	CdO	200	8	2.0 MPa and 864 K	B1-B2	P-Path	[5]
5	α-Fe_2O_3	200	11	2.0 MPa and 864 K	α-Fe_2O_3 to Fe_3O_4	K-path	[4]
6	Co_3O_4	150	12	2.0 MPa and 864 K	Co_3O_4 to CoO	K-path	[6]
7	α-MnO_2	200	14.81	2.0 MPa and 864 K	No transition	-	[7]
8	CeO_2	150	16.99	2.0 MPa and 864 K	No transition	-	[8]
9	α-Cr_2O_3	150	32.94	2.0 MPa and 864 K	No transition	-	[9]
10	SnO_2	200	35	2.0 MPa and 864 K	No transition	-	[10]
11	α-Al_2O_3	200	36	2.0 MPa and 864 K	No transition	-	[11]
12	NiO	200	46.02	2.0 MPa and 864 K	No transition	-	[12]
13	MgO	200	49.9	2.0 MPa and 864 K	No transition	-	[13]
14	ZnO	200	54	2.0 MPa and 864 K	No transition	-	[14]
15	CuO	200	69	2.0 MPa and 864 K	No transition	-	[15]
16	Nd_2O_3	200	-	2.0 MPa and 864 K	No transition	-	[16]
17	Sm_2O_3	200	-	2.0 MPa and 864 K	No transition	-	[17]

References

[1] S. Kalaiarasi, A. Sivakumar, S.A. Martin Britto Dhas, M. Jose, Shock wave induced anatase to rutile TiO_2 phase transition using pressure driven shock tube. Mater. Lett. 219, 72–75 (2018)

[2] S. Aswathappa, L. Dai, S. S. J. Dhas, R. S. Kumar, E. Palaniyasan, Size-dependent anatase to rutile phase transition under acoustic shocked conditions – A case study of TiO_2 bulk and nanoparticles. Appl. Surf. Sci. 681, 161501 (2025)

[3] S. Aswathappa, L. Dai, S. J. D. Sathiyadhas, R. S. Kumar, and M. V. Reddy, Acoustic shock wave-induced rutile to anatase phase transition of TiO_2 nanoparticles and exploration of their unconventional thermodynamic structural transition path of crystallization behaviors. Inorg. Chem. 63, 17043 17055 (2024)

[4] S. Aswathappa, A. Rita, S. S. J. Dhas, K. P. J. Reddy, R. S. Kumar, A. I. Almansour, S. Chakraborty, K. Moovendaran, J. Sridhar and S. A. M. B. Dhas, Dynamic shock wave driven simultaneous crystallographic and molecular switching between α-Fe_2O_3 and Fe_3O_4 nanoparticles – a new finding. Dalton Trans. 51, 9159–9166 (2022)

[5] S. Aswathappa, L. Dai, S. S. J. Dhas, S. A. M. B. Dhas, S. Laha, R. S. Kumar, and A. I. Almansour, Acoustic shock wave-induced solid-state fusion of nanoparticles: a case study of the conversion of one-dimensional rod shape into three-dimensional honeycomb nanostructures of CdO for high performance energy storage materials. Inorg. Chem. 63, 576 592 (2024)

[6] S. Aswathappa, S. Soundarya, S. S. J. Dhas, K. K. Bharathi, and S. A. M. B. Dhas, Shock wave driven solid state phase transformation of Co_3O_4 to CoO nanoparticles. J. Phys. Chem. C 124, 10755 10763 (2020)

[7] A. Rita, S. Aswathappa, S. Sahaya Jude Dhas, and S. A. M. B. Dhas, Reversible magnetic phase transitions of MnO_2 nano rods by shock wave recovery experiments. J. Mater. Sci: Mater. Electron 31, 20360–20367 (2020)

[8] A. Sivakumar, S. Ramya, S. S. J. Dhas, A. I. Almansour, R. S. Kumar, N. Arumugam, M. Murugesan, S.A. M. B. Dhas, Assessment of crystallographic and electronic phase stability of shock wave loaded cubic cerium oxide nanoparticles. Ceram. Int. 48, 1963–1968 (2022)

[9] E. D. Dona, A. Sivakumar, S. S. J. Dhas, P. Sivaprakash, S. Arumugam, S. A. M. B. Dhas, Sustainability of corundum-type Cr_2O_3 nanoparticles at shock wave loaded conditions. Solid State Sci. 119, 106701 (2021)

[10] S. Aswathappa, L. Dai, S. J. D. Sathiyadhas, R. S. Kumar, A. I. Almansour, S. Arumugam, M. Devaraj, and M. V. Reddy, Structural evolution of tin dioxide nanoparticles under acoustic shocked conditions for aerospace applications- implications of other rutile-type dioxides based on superheating approaches. ACS Appl. Nano Mater. 8, 17716 17730 (2025)

[11] S. Aswathappa, L. Dai, S. J. D. Sathiyadhas, R. S. Kumar, A. I. Almansour, M. Vijayan and R. Arul, Crystal structure response of corundum-type structures (α-Al_2O_3 and α-Fe_2O_3) under dynamic acoustic shocked conditions and comparison between static high-temperature and high-pressure conditions – Implications on volume-pressure-related phase transition types. (Communicated-2025)

[12] A. Rita, S. Aswathappa and S. A. M. B. Dhas, Investigation of structural and magnetic phase behaviour of nickel oxide nanoparticles under shock wave recovery experiment. J. Supercond. Nov. Magn. 33, 1845–1849 (2020)

[13] S. Aswathappa, L. Dai, S. J. D. Sathiyadhas, R. S. Kumar, A. I. Almansour, C. L. Selvakumar, V. V. Nallagounder and E. H. Modhi, Acoustic shock wave-induced crystal-structure and micro-structural stabilities of typical cubic lattice materials of MgO and CdO nanoparticles based on the superheating-melting approach. (Under review- 2025)

[14] S. Aswathappa, C. Victor, M. M. Nayak and S. A. M. B. Dhas, Structural, optical, and morphological stability of ZnO nano rods under shock wave loading conditions. Mater. Res. Express 6, 045031 (2019)

[15] S. Aswathappa, L. Dai, S. J. D. Sathiyadhas, R. S. Kumar, A. I. Almansour, C. L. Selvakumar, Acoustic shock wave-induced crystal-structure and micro-structural stabilities of CuO nanoparticles based on the superheating-melting approach. (Unpublished data)

[16] R. Sokkalingam, G. D. Raja, A. Panghal, S. S. Roy, E. M. Sankaran, B. A. Arumugam Sonachalam, Enhancing photocatalytic dye degradation efficiency through the utilization of shock wave effects on neodymium oxide (Nd_2O_3). J. Mol. Struct. 1318, 139215 (2024)

[17] R. Sokkalingam, A. Panghal, S. S. Roy, E. M. Sankaran, A. Sonachalam, Impact of shockwaves on the structural and morphological characteristics of the Sm_2O_3 compound for wastewater treatment. J. Taiwan Inst. Chem. Eng. XX, 106105 (2025)